steel research international
www.steel-research.de

Constrained Equilibrium Reactions in a Low Carbon Steel During Heat Treatments Below the M_S

Felipe M. Castro Cerda, Constantinos Goulas, Eliseo I. Hernández, Juan P. Sanhueza, Tanya Ros-Yanez, and Roumen H. Petrov*

Isothermal heat treatments below the martensite start temperature are carried out in a 0.25C-1.4Mn-1.4Si-0.32Mo steel (in wt%). The microstructural observation reveals a combination of tempered lath and plate martensite, accompanied by bainite and retained austenite. The temperature variation of the austenitic carbon content under different constrained equilibrium models is calculated and compared with experimental measurements. Neither of the existing models seems to predict the behavior of the measured austenitic carbon content in the temperature range studied. The results suggest that the diffusional formation of bainite governs the carbon content of austenite at temperatures nearby the M_S.

1. Introduction

The quenching and partitioning of steels aim for obtaining a microstructure of martensite and austenite at room temperature. To produce such a phase mixture, the thermal cycle usually applied consists of quenching the sample from the fully austenitic range to a temperature between M_S and M_F, and then giving a holding time at the same temperature or higher. During this time, known as partitioning time, the carbon from martensite diffuses to the untransformed austenite. The goal is to produce a final microstructure consisting of a specific combination of martensite and stabilized austenite, which delivers outstanding mechanical performance, combining strength in the range above 1 GPa, and elongation at fracture above 15%.[1]

Perhaps the most important parameter for the design of suitable Q&P compositions is the prediction of the fraction of stabilized austenite at room temperature for a given thermal path. The existing thermodynamic models[2–4] have provided a simplified framework of predictions with a reasonable degree of accuracy under specific conditions. However, such models do not take into account, for example, the presence of bainite and the equilibrium deviation due to the strain energy in their calculations. The aim of the present study is to explore such models, to test whether or not they can properly describe the phase evolution below the M_S. The predictions are compared with X-ray diffraction-based experimental measurements and in-depth SEM-based microstructural characterization. The results are discussed on the basis of the existing thermodynamic descriptions of the phases and constituents observed experimentally, which are described in detail in the next section.

2. Phase Equilibria During Quenching and Partitioning

2.1. Austenite–Martensite Equilibrium

The stabilization of austenite occurs by virtue of carbon enrichment, which diffuses from martensite due to the existing chemical driving force. Speer et al.[2,3] provided a thermodynamic description of the endpoint of carbon redistribution, although subsequently amended.[5–7] Their proposal, termed as constrained carbon equilibrium (CCE), considers that the equilibrium between martensite and austenite of the same initial chemical composition consists only on the redistribution of carbon atoms, i.e., iron atoms do not diffuse. The construction of a Gibbs free energy versus composition diagram will readily show that there is no unique solution for this condition. Therefore, Speer et al. introduced the mass balance of carbon, for which

F. M. Castro Cerda, E. I. Hernández
Department of Metallurgy
University of Santiago de Chile
Alameda 3363, Estación Central, Santiago 9170022, Chile
E-mail: felipe.castro@usach.cl

C. Goulas
Faculty of Engineering Technology (ET)
Department of Design, Production, and Management
University of Twente
Drienerlolaan 5, 7500AE Enschede, The Netherlands

E. I. Hernández, R. H. Petrov
Department of Electromechanical Systems and Materials, Research Group Materials Science and Technology
Ghent University
Tech Lane Science Park Campus A 46, Gent, Belgium

J. P. Sanhueza
Departamento de Ingeniería de Materiales
Universidad de Concepción
Edmundo Larenas 270, Concepción 4070415, Chile

T. Ros-Yanez
Research & Innovation Center
Cleveland-Cliffs Inc.
6180 Research Way, Middletown, OH 45005, USA

R. H. Petrov
Department of Materials Science and Engineering
Delft University of Technology
Mekelweg 2, 2628CD Delft, The Netherlands

The ORCID identification number(s) for the author(s) of this article can be found under https://doi.org/10.1002/srin.202200841.

DOI: 10.1002/srin.202200841

$$X_C^{\alpha'} \times f_V^{\alpha'} + X_C^{\gamma} \times f_V^{\gamma} = X_C^{0} \quad (1)$$

where X_i^k is mole fraction of i in the phase k and f_V^k is volume fraction of the phase k. X_C^0 represents the initial composition of the system in mole fraction. The accurate prediction of the austenitic carbon content stems on the correct assessment of thermodynamic data at low temperatures (conveniently performed by computational databases), the correct prediction of the M_S, and the temperature variation of the martensitic phase fraction. There is a considerable number of empirical and phenomenological relations for the estimation of M_S summarized elsewhere,[8–10] and models for determining the phase fraction of martensite.[11–13] One drawback of CCE is that it does not take into account for precipitation of carbides in martensite during the partitioning stage.

2.2. Austenite–Martensite–Cementite Equilibrium

Toji et al.[4] proposed that the constrained equilibrium is to consider the carbide precipitation in martensite (called constrained carbon equilibrium with cementite precipitation, CCEθ) and to compute the carbon redistribution in austenite henceforth. The condition of equilibrium is that the chemical potential of carbon is the same in all phases. This can be expressed as

$$\mu_C^{\alpha'} = \mu_C^{\theta} = \mu_C^{\gamma} \quad (2)$$

Experimental observations have shown that the tempering of martensite is virtually unavoidable during the partitioning stage,[4,14–17] despite the addition of Si.[16] CCEθ model[4] does not account for the mass balance of carbon. A recent model[18] combining key aspects of both previous models, namely the equilibrium between martensite, carbide, and austenite; and the balance of carbon content among the phases is expressed by the following equality

$$X_C^{\alpha'} \cdot f_V^{\alpha'} + X_C^{\theta} \cdot f_V^{\theta} + X_C^{\gamma} \cdot f_V^{\gamma} = X_C^{0} \quad (3)$$

2.3. Austenite–Bainite Equilibrium

The equilibria described in the previous sections deal with so-called "endpoints" of a constrained state. The mechanism whereby these final states are accomplished is disregarded in the mass balance relations proposed. Although a recent study by Dai et al.[19] explores the local equilibrium conditions at the α_M/γ interface, in the interpretation of their results they seem to ignore both carbide precipitation in martensite and the formation of bainite (for which they provide experimental evidence). The equilibrium which takes place in the α_B/γ interface during bainite formation, which is dynamic and depends on the local conditions at the interface, determines the carbon content in austenite. The diffusionless approach to the mechanism of bainite formation postulates that the movement of the α_B/γ interface is controlled by the stepwise nucleation of subunits,[20] defining a temperature dependence of the carbon content in austenite given by the so-called T_0' line.[21] Whenever the composition of austenite nearby the α_B/γ interface reaches T_0', the transformation cannot proceed further. The diffusional paradigm of bainitic growth[22,23] proposes that the advance of the α_B/γ interface is controlled by the diffusion of carbon in austenite. It predicts a limiting carbon content in austenite at the tip of the plate according to the so-called WB_S.[22]

The formation of bainite below the M_S is well documented in the recent literature.[24–27] It is, thus, reasonable to expect that bainite formation will have an impact upon the stability of austenite during the isothermal transformation.

3. Experimental Section

A steel grade with a composition shown in **Table 1** was produced in a vacuum induction furnace. The average carbon content in mole fraction is 1.15E-2. The $130 \times 130 \times 200\,mm^3$ slabs were reheated to 1523 K and hot-rolled in multiple passes to a final thickness of 13 mm. The heat treatments were performed on a Bähr 805A Quench dilatometer on cylindrical samples of $10 \times 5\,mm^3$ (length × diameter) taken out at approximately 2/3 of hot rolled steel plate thickness, with the long axis of the sample oriented parallel to the plate transverse direction. The thermal cycles are shown in **Figure 1**a, and consisted of four steps as follows: 1) homogenization of the austenite in the specimens in the fully austenitic range (1173 K for 120 s), 2) quenching at three different temperatures between M_S and M_F, 3) isothermal holding for 600 s (or 300 s) at the quench temperature, and 4) quenching to room temperature. The parameters of the heat treatments are shown in **Table 2**. The sample nomenclature shows in first place the quenching temperature (QT) in K, second, the isothermal holding time (Ht) in s at the quenching temperature, third, the partitioning temperature (PT) in K, and fourth, the partitioning time (Pt) in s at the partitioning temperature. Figure 1b shows a second thermal cycle, which includes the partitioning stage at a temperature higher than the quenching temperature. The quenching temperature was held constant at 548 K for 300 s, followed by a partitioning at 573 and 673 K for 600 s.

4. Analysis

The data analysis was carried out according to the same methodology of a previous study.[28] The temperature variation of phase fractions was calculated by applying the lever rule to the dilatometric curves. The microstructural evolution of the samples was characterized via scanning electron microscopy (SEM). Samples were prepared in the middle of each heat-treated specimen, next to the place where the thermocouple was welded and the characterization was carried out in TD plane. Samples taken from each tested specimen were prepared, in accordance to the standard procedure, by grinding and polishing to a mirror-like finish using a 1 μm diamond paste and etching to reveal the microstructure. The polished surface was swabbed in a solution of 4% v/v HNO_3 in ethanol (nital 4%) for ≈4 s. Thermodynamic

Table 1. Chemical composition of the steel samples in wt%.

C	Mn	Si	P	S	Mo	Ti	Nb	Al	Fe
0.25	1.48	1.44	0.006	0.004	0.32	0.02	0.035	0.02	rest

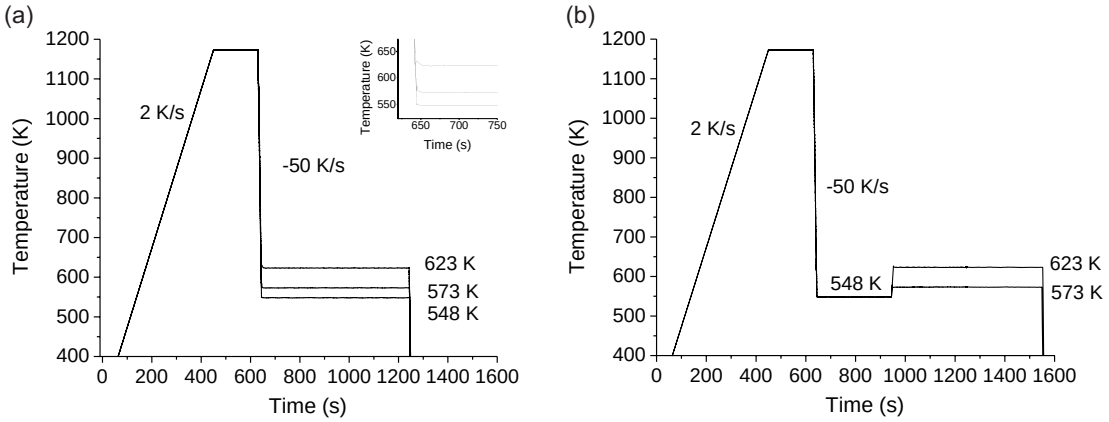

Figure 1. Schematic representation of the single a) and two-stage b) isothermal heat treatments used in this work.

Table 2. Parameters of the heat treatments.

QT/Ht/PT/Pt	Quenching temp. [K]	Isothermal time [s]	Partitioning temp. [K]	Isothermal time [s]	Final cooling [K s^{-1}]
548/600	548	600	–	–	−50
573/600	573	600	–	–	−50
623/600	623	600	–	–	−50
548/300/573/600	548	300	573	600	−50
548/300/623/600	548	300	623	600	−50

calculations were carried out with the software ThermoCalc, database TCFE9.

Austenite volume fractions and the austenite lattice parameter were determined from X-ray diffraction (XRD) analysis. XRD measurements were carried out using a Bruker D8 Advance Diffractometer, equipped with coradiation ($K\alpha_1 = 1.78897$ Å) operating at 45 kV and 35 mA in Bragg–Brentano mode with sample spinning at 30 rpm. The angular range 2θ between 30° and 130° was scanned with a step size of 0.021° and dwell time of 2 s/step. The retained austenite volume fractions were obtained as per the direct comparison method outlined in Ref. [29]

$$f_V^{\gamma} = \frac{\frac{1}{n_{FCC}}\sum_0^n \left(I_{FCC}^{hkl} \Big/ R_{FCC}^{hkl} \right)}{\frac{1}{n_{FCC}}\sum_0^n \left(I_{FCC}^{hkl} \Big/ R_{FCC}^{hkl} \right) + \frac{1}{n_{BCC}}\sum_0^n \left(I_{BCC}^{hkl} \Big/ R_{BCC}^{hkl} \right)} \quad (4)$$

where $I^{hkl}{}_i$ is the integrated intensity of the phase i measured for a single preselected diffracted plane or "peak" (FCC: {200}, {220}, {311}; BCC: {200}, {211}, {220}). The factor $R^{hkl}{}_i$ corresponds to the theoretical intensity of the phase i for the above-indicated planes and n_k is the number of used peaks of the phase i.

The FCC lattice parameter (a^{γ}, in 1E-10 m) was calculated using the Nelson–Riley method considering the aforementioned FCC planes.[30] Subsequently, the carbon content of austenite, $X_C{}^{\gamma}$ (in at%) was estimated according to the equation proposed by Cheng et al.[31] for unstrained austenite following the analysis by Scott and Drillet.[32]

$$a^{\gamma} = 0.3573 + 0.00075X_C^{\gamma} \quad (5)$$

The methodology for calculating the carbon content of austenite according to the three constrained equilibrium models (CCE, CCEθ, and BCEθ), and the carbon content of austenite in equilibrium with bainite according to the diffusional and displacive paradigms (WB_S and T_0', respectively) is described in detail in a previous work.[28]

5. Results

Figure 2 shows the microstructure of one-step heat treatment samples quenched at 548, 573, and 623 K. The three quenching temperatures are lower than the M_S (≈653 K). The microstructure at 548 K consists mainly of martensite areas and tempered carbides (white thin strips within martensitic areas). At 573 K, also lower bainite is observed (cf. white LB arrows in Figure 2b,e), whereas at 623 K both upper (cf. white UB arrows in Figure 2c,f) and lower bainite are clearly resolved. Lower and upper bainite show the typical morphological characteristics of these constituents. In the former, carbide precipitation takes place within the bainitic plates, whereas in the latter the precipitation is observed between plates. The bright white zones between martensitic laths or upper bainitic plates are associated with retained austenite.

The martensitic start temperature and the temperature variation of the volume fraction of martensite were experimentally measured via dilatometry (**Figure 3**c). The transformed fractions of martensite at each quenching temperature are 0.90, 0.78, and 0.18 for 548, 573, and 623 K, respectively. Figure 3d shows the change in length during the isothermal holding. It is observed that the lengthening of the dilatometry sample decreases with temperature. X-ray diffraction measurements (**Figure 4**) allowed the determination of the fraction of retained austenite (RA) and the average carbon content in austenite. The results are shown in **Table 3**. There is a clear decrease of the RA fraction from 0.082 to 0.051 as the quenching temperature is raised. Conversely, the carbon content of austenite increases monotonically from 0.046 to 0.066 mol. fraction with the quenching temperature.

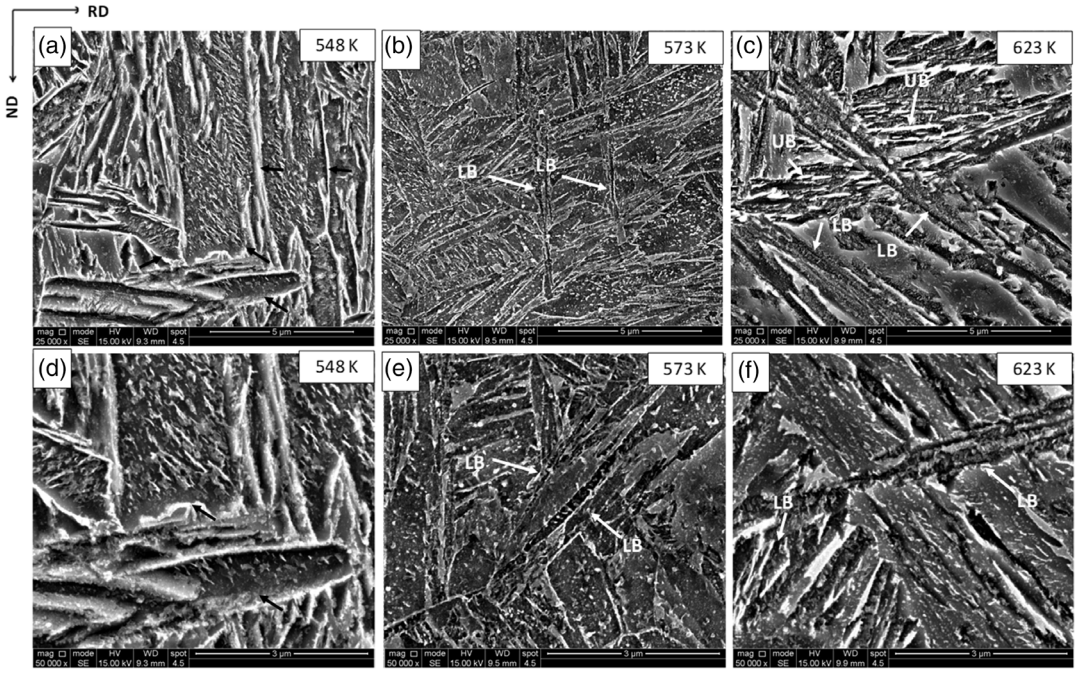

Figure 2. The microstructures after one-step heat treatments. The temperature of the heat treatments is shown in the upper-right corner of each image. Mostly martensite is observed in (a,d), whereas a mixture of martensite and bainite (LB and UB, lower and upper bainite, respectively) is shown in (b,e) and (c,f). Etched with nital 4%, scale bars are 5 μm (a–c) and 3 μm (d–f).

6. Discussion

6.1. The Evolution of the Microstructure

The morphology of martensite transformed during heat treatments is consistent in the three experimental conditions. Tempered lath martensite is the most observed, whereas plate martensite is also observed. **Figure 5** shows areas of mixed plate/lath martensite at the three temperatures. Typically, the plate of martensite (white arrows) which formed first is later surrounded by lath martensite,[33] displaying a rather characteristic overall shape that is often referred as "lenticular." Two morphologies of carbide are observed, thin elongated and a roundish (cf. Figure 5a,b). The former is associated with low-temperature precipitation of either cementite or Hägg carbide, and displays a cylindrical shape.[34] The latter is usually cementite, which might have grown drawing carbon from less stable cylindrical precipitates.[34] It is observed that the precipitation of carbides is not uniform in the bulk, since there are zones nearby the martensitic boundaries in samples quenched to 548 K (cf. black arrows in Figure 2a,d) in which no precipitation is observed. This observation has been previously reported and discussed elsewhere,[28] and it is suggested that the growth of carbides at the α_M/γ interface during the isothermal holding could explain the rim of fresh martensite formed during the final cooling.

A qualitative inspection of the microstructure (cf. Figure 2) indicates that there is a significant fraction of bainite close to the M_S (623 K), which seems to decrease at lower quenching temperatures. Figure 2c,f, which corresponds to QT = 623 K, displays a large fraction of both UB and LB. At QT = 573 K (cf. Figure 2b,e), only a few scattered plates of LB are observed. Bainite is not resolved at QT = 548 K. The metallographic observations are consistent with the dilatometric data and X-ray diffraction measurements. Figure 3b also shows that there is considerable lengthening of the samples at 623 and 573 K, whereas the lengthening is negligible at 548 K. **Table 4** shows the amount of phase available for transforming both isothermally to bainite and into fresh martensite upon cooling. At 623 K, the austenite fraction available for transformation is ≈0.82, whereas at 548 K is only ≈0.1. A large fraction of bainite at a temperature near the M_S would thus be possible.

6.2. The Prediction of Austenitic Carbon Content Under $\alpha_M/\theta/\gamma$ Equilibrium

When considering either CCE or BCEθ models, one could reasonably expect that the carbon content in austenite increases with respect to the initial composition after partitioning. The degree of carbon enrichment in austenite will depend on the phases considered in the equilibrium. CCE will produce a more considerable enrichment than BCEθ because the latter includes cementite precipitation in martensite. CCE prediction becomes significantly higher (around one order of magnitude) than BCEθ at lower temperatures. Toji et al.[4] showed that the CCEθ prediction of carbon content in austenite is virtually constant, regardless of the fraction of martensite. A calculation of the carbon content of austenite in equilibrium with martensite under CCE, CCEθ, and BCEθ considering the composition of the studied steel is shown in **Figure 6**. The calculations were carried out with the software ThermoCalc, version 2020a, database TCFE9. The M_S temperature was calculated according to Wang et al.[8] It is observed that

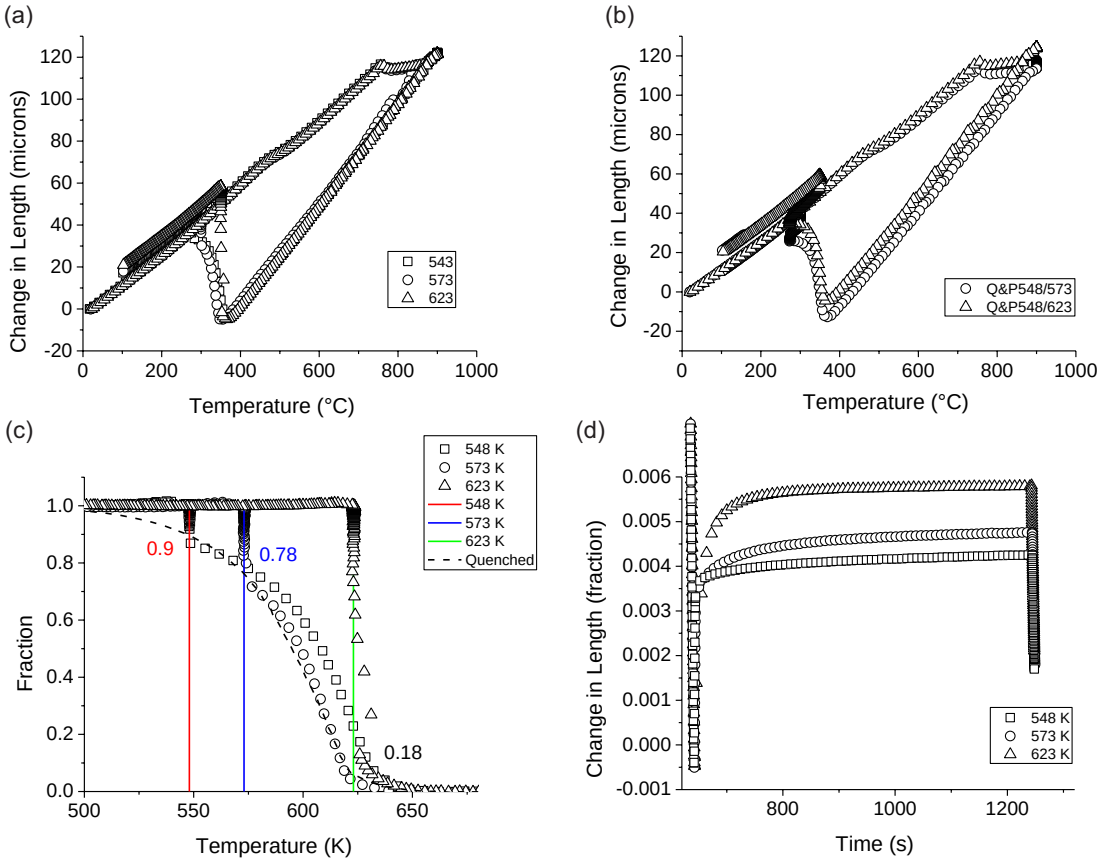

Figure 3. Results of the dilatometric tests. a) Isothermal one-step experiments, b) isothermal two-step experiments, c) calculated temperature variation of the transformed martensite fraction, and d) change in length occurring during the isothermal holding.

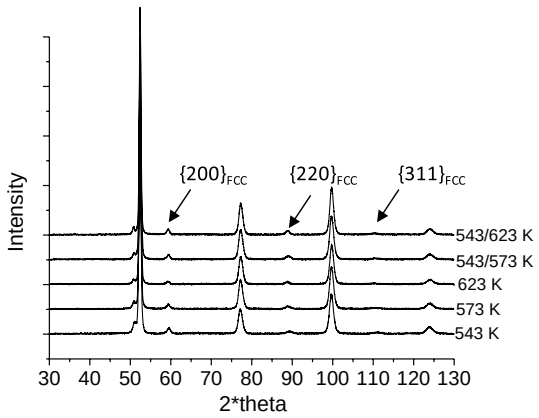

Figure 4. X-ray diffraction results. Arrows highlight the peaks of austenite used in the calculations.

the three models produce quite different degrees of carbon enrichment in austenite. It is graphically clear that CCE predicts an austenitic carbon content that quickly stabilizes γ against further martensitic transformation on cooling, whereas CCEθ model yields a virtually constant ≈0.08 mol. fraction of carbon in austenite.

Table 3. Data on volume fraction of retained austenite (RA) and its carbon content (mol. fraction).

QT/Ht/PT/Pt	Vol. fr. of austenite	Mol. fr. of C in austenite[30]
548/600	0.082 (0.01)	0.046
573/600	0.073 (0.01)	0.057
623/600	0.051 (0.01)	0.066
548/300/573/600	0.076 (0.01)	0.056
548/300/623/600	0.075 (0.01)	0.062

BCEθ predicts a carbon enrichment of austenite which might still allow for fully martensitic transformation at room temperature, depending on the isothermal holding temperature. For example, if a sample is quenched to 573 K (≈300 °C), the predicted carbon content of austenite after partitioning (0.018 in mole fr. of C) will be at the left-hand side of the M_S at room temperature (located ≈0.044 mole fr. of C, according to the formula of Wang et al.),[8] hence, it is likely to form fresh martensite upon cooling. The same holds for any austenite composition at the left-hand side of 0.044 in mole fr., in the ideal case that the only phases involved in the equilibrium are martensite, austenite, and cementite (or any other carbide). BCEθ model of carbon enrichment in austenite predicts that austenite at 548, 573, and 623 K

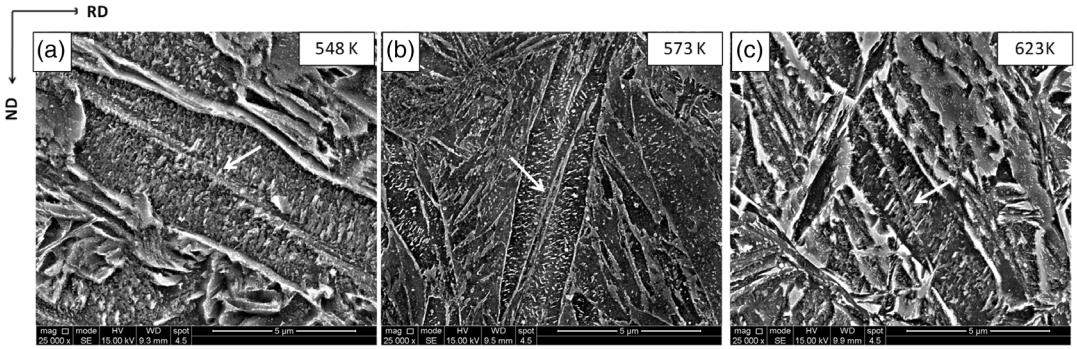

Figure 5. Mixed plate/lath martensite zones. White arrows indicate the midrib in plate martensite. The temperature of the heat treatments is shown in the upper-right corner of each image a) 548 K, b) 573 K, and c) 623 K. Etched with nital 4%, scale bars are 5 μm.

Table 4. Phase distribution after heat treatments.

QT	Martensite fr.	Retained austenite fr.	Other[a)]
623	0.18	0.08	0.74
573	0.78	0.07	0.15
548	0.90	0.05	0.05

[a)]Transformed to bainite and/or fresh martensite.

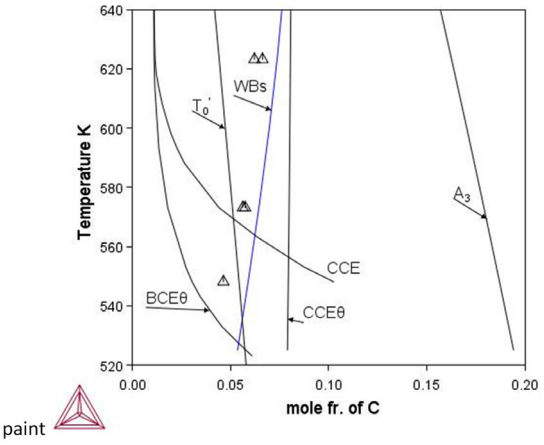

Figure 6. An isopleth section of the phase diagram. The triangles denote experimental points measured via X-ray diffraction.

could still form fresh martensite on cooling, thereby explaining the outer rim of nontempered martensite (arrows) observed in Figure 2. If, for instance, the same system is quenched at a temperature at which BCEθ predicts a carbon content in austenite $\geq$0.044 mole fr. (i.e., at the right-hand side of the dashed red line in Figure 5), the degree of carbon enrichment of austenite is likely to stabilize it at room temperature. The ideal quenching temperature for quenching the studied system would be ≈537 K (264 °C). Notice that the martensitic fraction at this temperature, according to the dilatometry tests, is ≈0.93. Quenching to this temperature allows theoretically to stabilize only 0.07 of the total volume as austenite, which coincides with the experimental data on RA, as shown in Table 4.

The experimental data show that the carbon content in austenite decreases with the temperature. The values seem to fall close to the CCEθ prediction nearby the M_S, whereas approaching toward BCEθ prediction at low temperatures. It should be noted that none of the existing $\alpha_M/\theta/\gamma$ constrained equilibrium models describe the positive slope of the experimental temperature dependence of carbon content in austenite.

6.3. The α_B/γ Equilibrium

Figure 2 revealed the presence of bainite at 573 and 623 K (300 and 350 °C). The experimental carbon content in austenite shows large deviations from the CCE, CCEθ, and BCEθ models at these temperatures (see Figure 6), which are consistent with the observation of bainite in the microstructure. Is to be noticed that the carbon content in austenite at both temperatures lies at the right-hand side of T_0' line, which is the theoretic limit imposed by the displacive paradigm of bainitic transformation. The results suggest that bainite could not have been formed under diffusionless growth of subunits. Conversely, the experimental data seem to fit fairly well with the WB_S prediction, even at 548 K.

Two additional quenching tests at 548 K (275 °C), followed by partitioning at 573 K (300 °C), and 623 K (350 °C) for 600 s were carried out to test whether the carbon content in austenite was determined by the initial martensitic fraction $f_V^{\alpha'}$ (cf. Equation (3)) or the local equilibrium conditions at the partitioning temperature. The results are shown in Table 3. Despite the fact that $f_V^{\alpha'}$ is roughly 0.90 for quenching at 548 K (275 °C) and 0.18 for quenching at 623 K (350 °C), the carbon content in austenite is virtually the same for 623 K (350 °C) partitioning temperature, within the spread of the measurement. A similar conclusion is made when comparing single-step partitioning at 573 K (300 °C) with the sample quenched at 548 K (275 °C) and partitioned at 573 K (300 °C), for which $f_V^{\alpha'}$ is different by a factor of ≈ 3. The results suggest that the local equilibrium at the α_B/γ interface plays a major role on the carbon content of austenite at 573 K (300 °C) and 623 K (350 °C). The present findings are consistent with the results of a previous study.[28] It is interesting to compare the former discussion with the results of the simulation study by Dai et al.,[19] whereby NPLE conditions deliver carbon contents in austenite almost independent of QT. Although not discussed by Dai et al.,[19] NPLE

conditions are likely to establish during diffusional growth of bainitic ferrite.[35,36] The predicted carbon content of austenite nearby the α_B/γ interface might be different to their calculations due to the kinetic factor associated to the curvature of the interface.

6.4. Deviation from the Predictions at Low Temperatures

Despite that bainite was not observed in the sample quenched at 548 K (275 °C), Figure 5 shows a noticeable deviation of the experimental data from CCE, CCEθ, and BCEθ models. The origin of this deviation is as yet not fully understood. The simplest explanation could be that bainite is still formed at 548 K, yet it was not detected by SEM analysis. Bainite formation may explain the carbon content of austenite at low temperatures due to the reasonable fitting of the experimental data in Figure 2 either with the T_0' or WB_S curve.

7. Conclusions

Isothermal heat treatments on 0.25C-1.4Mn-1.4Si-0.32Mo steel have been carried out at temperatures below the M_S. The results suggest that the final carbon content of austenite at 623 and 573 K are not determined by any of the existing $\alpha_M/\theta/\gamma$ constrained equilibrium models. It is likely that the α_B/γ equilibrium is playing the major role in determining the final carbon content in austenite, hence its stability.

Likewise, the combination of single and two-step partitioning experiments indicates that the initial fraction of martensite formed below M_S ($f_V^{\alpha'}$) is not a relevant factor to define the stability of austenite, whenever bainite is present in the microstructure (623 and 573 K for the case of the present experimental conditions).

BCEθ model predicts that austenite after isothermal heat treatments at 548, 573, and 623 K can further transform into fresh martensite upon cooling.

The carbon content of austenite at 623 and 573 K is higher than the predictions of T_0', which suggests that bainite could have not formed according to the diffusionless paradigm. Conversely, the results seem to fit the WB_S prediction with reasonable accuracy, supporting the diffusional paradigm for bainitic formation.

Acknowledgements

F.M.C.C. acknowledges the support of the National Agency for Research and Development (ANID), Project No. 1220058. E.I. Hernandez acknowledges the support of National Agency for Research and Development (ANID)/Doctorado Nacional/2017-21171319. C.G. acknowledges funding from the Dutch organization for scientific research (NWO-Nederlandse Organisatie voor Wetenschappelijk Onderzoek) in the framework of project GradWAAM, project number S16043.

Conflict of Interest

The authors declare no conflict of interest.

Data Availability Statement

The data that support the findings of this study are available from the corresponding author upon reasonable request.

Keywords

austenite, constrained equilibrium, martensite, quenching and partitioning, stabilization

Received: November 3, 2022
Revised: March 3, 2023
Published online:

[1] E. De Moor, P. J. Gibbs, J. G. Speer, D. K. Matlock, A. S. Processing, *AIST Trans.* **2015**, *7*, 2010.
[2] J. Speer, D. K. Matlock, B. C. De Cooman, J. G. Schroth, *Acta Mater.* **2003**, *51*, 2611.
[3] J. G. Speer, D. V. Edmonds, F. C. Rizzo, D. K. Matlock, *Curr. Opin. Solid State Mater. Sci.* **2004**, *8*, 219.
[4] Y. Toji, G. Miyamoto, D. Raabe, *Acta Mater.* **2015**, *86*, 137.
[5] M. Hillert, J. Ågren, *Scr. Mater.* **2004**, *50*, 697.
[6] J. G. Speer, D. K. Matlock, B. C. DeCooman, J. G. Schroth, *Scr. Mater.* **2005**, *52*, 83.
[7] M. Hillert, J. Ågren, *Scr. Mater.* **2005**, *52*, 87.
[8] J. Wang, P. J. van der Wolk, S. van der Zwaag, *Mater. Trans. JIM* **2000**, *41*, 761.
[9] T. Sourmail, C. Garcia-Mateo, *Comput. Mater. Sci.* **2005**, *34*, 323.
[10] A. Stormvinter, A. Borgenstam, J. Ågren, *Metall. Mater. Trans. A* **2012**, *43*, 3870.
[11] D. P. Koistinen, R. E. Marburger, *Acta Metall.* **1959**, *7*, 59.
[12] S.-J. Lee, C. J. Van Tyne, *Metall. Mater. Trans. A* **2012**, *43*, 422.
[13] F. Huyan, P. Hedström, A. Borgenstam, *Mater. Today Proc.* **2015**, *2*, S561.
[14] F. Hajy Akbary, J. Sietsma, G. Miyamoto, T. Furuhara, M. J. Santofimia, *Acta Mater.* **2016**, *104*, 72.
[15] D. T. Pierce, D. R. Coughlin, D. L. Williamson, J. Kähkönen, A. J. Clarke, K. D. Clarke, J. G. Speer, E. De Moor, *Scr. Mater.* **2016**, *121*, 5.
[16] B. Kim, J. Sietsma, M. J. Santofimia, *Mater. Des.* **2017**, *127*, 336.
[17] D. T. Pierce, D. R. Coughlin, K. D. Clarke, E. De Moor, J. Poplawsky, D. L. Williamson, B. Mazumder, J. G. Speer, A. Hood, A. J. Clarke, *Acta Mater.* **2018**, *151*, 454.
[18] F. M. Castro Cerda, C. Goulas, L. A. I. Kestens, *Metall. Mater. Trans. A* **2021**, *52*, 2155.
[19] Z. Dai, R. Ding, Z. Yang, C. Zhang, H. Chen, *Acta Mater.* **2018**, *144*, 666.
[20] J. M. Oblak, R. F. Hehemann, in *Transformation and Hardenability in Steels*, Climax Molibdenum Company of Michigan, Ann Arbor, MI, **1967**.
[21] H. K. D. H. Bhadeshia, *Bainite in Steels*, Maney Publishing, Wakefield, UK **2015**.
[22] M. Hillert, Intern. Rep. Swedish Inst. Met. Research **1960**.
[23] L. Kaufman, S. V. Radcliffe, M. Cohen, in *Decomposition of Austenite by Diffusional Processes* (Eds.: V.F. Zackay, H.I. Aaronson), The Metallurgical Society of AIME, London **1962**, pp. 313–352.
[24] S. M. C. van Bohemen, M. J. Santofimia, J. Sietsma, *Scr. Mater.* **2008**, *58*, 488.
[25] P. Kolmskog, A. Borgenstam, M. Hillert, P. Hedstrom, S. S. Babu, H. Terasaki, Y. I. Komizo, *Metall. Mater. Trans. A* **2012**, *43*, 4984.
[26] S. Samanta, P. Biswas, S. Giri, S. B. Singh, S. Kundu, *Acta Mater.* **2016**, *105*, 390.

[27] A. Navarro-López, J. Hidalgo, J. Sietsma, M. J. Santofimia, *Mater. Charact.* **2017**, *128*, 248.
[28] F. M. Castro Cerda, E. I. Hernández, T. Ros-Yanez, R. H. Petrov, *Metall. Mater. Trans. A* **2020**, *51*, 1506.
[29] C. F. Jatczak, *SAE Trans.* **1980**, *89*, 1657.
[30] L. Cheng, A. Bottger, T. H. Keijser, E. J. de Mittemeijer, *Scr. Metall. Mater.* **1990**, *24*, 509.
[31] C. P. Scott, J. Drillet, *Scr. Mater.* **2007**, *56*, 489.
[32] J. B. Nelson, D. P. Riley, *Proc. Phys. Soc.* **1945**, *57*, 160.
[33] A. Shibata, S. Morito, T. Furuhara, T. Maki, *Acta Mater.* **2009**, *57*, 483.
[34] G. R. Speich, *Trans. AIME* **1969**, *245*, 2553.
[35] M. Hillert, *Metall. Mater. Trans. A* **1994**, *25*, 1957.
[36] M. Hillert, *J. Alloys Compd.* **2001**, *320*, 161.